Monolithic on-chip nonreciprocal photonics based on magneto-optical thin films

Juejun Hu*, Xue Yin Sun, Qingyang Du, Mehmet Onbasli, and Caroline. A. Ross*
Department of Materials Science and Engineering
Massachusetts Institute of Technology
Cambridge MA, 02139, USA

ABSTRACT

Monolithic integration of nonreciprocal optical devices on semiconductor substrates has been a long-sought goal of the photonics community. One promising route to achieve this goal is to deposit high quality magneto-optical (MO) oxide thin films directly on a semiconductor substrate. In this article, we will review our ongoing progress in material development and device engineering towards enabling a monolithically integrated, high-performance magneto-optical nonreciprocal photonics platform. In particular, we will discuss our recent work which has led to a new pulsed laser deposition (PLD) technique of Ce or Bi substituted yttrium iron garnet (YIG) thin films with reduced thermal budget, simplified growth protocols and improved magneto-optical characteristics. These materials were incorporated in monolithic resonator and interferometer based isolator devices to demonstrate on-chip optical isolation with improved device figure of merit. Challenges and opportunities for monolithic magneto-optical devices will be discussed in the context of our latest material and device performance metrics.

KEY WORDS: Magneto-optical isolator, magnetic garnets, silicon photonics, photonic integration

1. NONRECIPROCAL PHOTONICS: AN OVERVIEW

Nonreciprocal photonic devices exemplified by optical isolators and circulators are essential components for optical interconnects for both telecommunications and data communications. As the counterpart of electrical diodes in photonics, isolators and circulators play a critical role in PICs by preventing harmful feedback between different parts of the circuit. For example, an isolator is often used to protect a laser source from destabilizing feedback or damage from back-reflected light. The need for on-chip isolation becomes imperative as the level of photonic integration continues to scale, since unwanted reflections between the many integrated devices are very common and can be highly disruptive in a complex optical network. With the development of integrated lasers, waveguides, modulators and detectors, the isolator is becoming the missing component in a fully integrated photonic circuit.

Fundamentally, optical isolation requires breaking the time-reversal symmetry of light propagation. Such optical nonreciprocity can be realized by using magnetooptical (MO) effects or non-magnetic approaches such as indirect interband photonic transitions[1] and nonlinear optics[2, 3]. Traditional optical isolators used in free-space and fiber-optic

*hujuejun@mit.edu, phone: 1-302-766-3083; caross@mit.edu, phone: 1-617-258-0223, fax: 1-617-252-1020

Integrated Optics: Devices, Materials, and Technologies XX, edited by Jean-Emmanuel Broquin, Gualtiero Nunzi Conti, Proc. of SPIE Vol. 9750, 97500W · © 2016 SPIE
CCC code: 0277-786X/16/$18 · doi: 10.1117/12.2209658

Downloaded From: http://proceedings.spiedigitallibrary.org/ on 02/07/2017 Terms of Use: http://spiedigitallibrary.org/ss/termsofuse.aspx

systems are almost exclusively based on Faraday rotation in MO crystals. These Faraday rotation isolators typically feature an isolation ratio of the order of 30 to 40 dB, an insertion loss below 1 dB, and an operation bandwidth exceeding 50 nm in the telecommunication window[4, 5]. Despite the high performance of these free-space isolators, they are bulky discrete devices not suitable for planar on-chip integration. In addition, at present the price of a discrete isolator ranges anywhere from $30 up to over $1,000, a prohibitive cost for large-scale PICs.

Development of on-chip isolators has been hampered by the incompatibility of traditional MO materials with monolithic integration on semiconductor substrate platforms. Unlike doped-glass-based fiber-optic isolators, the very limited real estate on a chip requires the use of materials with high Verdet constants (i.e. large Faraday rotation) in on-chip isolators. These materials, typically single-crystalline bismuth or cerium doped yttrium iron garnet (Bi:YIG, $Bi_xY_{3-x}Fe_5O_{12}$ and Ce:YIG, $Ce_xY_{3-x}Fe_5O_{12}$), cannot be monolithically grown on common semiconductor substrates (Si or InP) due to large lattice and thermal expansion mismatch[6].

Two routes have been pursued to resolve the integration challenge: the hybrid approach which relies on wafer bonding of garnet crystals[7-11], and the monolithic approach which directly deposits polycrystalline ferromagnetic oxides or doped semiconductors/polymers[12-15] on semiconductor substrates. The former approach can leverage the large Verdet constant and low material absorption in single-crystalline garnets to achieve good isolation performance; however, the wafer bonding process required by this approach can limit fabrication throughput and yield. Doped semiconductors and polymers can be readily integrated with semiconductors, although they often suffer from high optical loss (1000 dB/cm and above) due to incorporation of highly absorptive metallic iron[16, 17]. Deposited polycrystalline ferromagnetic oxides is an alternative material system for monolithic nonreciprocal device integration as we will discuss in the next sections.

On-chip magnetooptical isolation based on these MO oxides can be achieved by Faraday rotation, nonreciprocal loss, nonreciprocal mode conversion/cut-off/coupling, as well as nonreciprocal phase shift (NRPS). In a Faraday rotator, a magnetic field is applied along the light propagation direction to induce circular birefringence and hence polarization rotation. This configuration, however, is very sensitive to waveguide birefringence and is not suitable for on-chip isolation[18, 19] unless a quasi-phase match scheme is implemented[20]. Shimizu *et al.* demonstrated nonreciprocal optical loss in an InGaAsP waveguide coated on a sidewall with iron showing an isolation ratio of 14.7 dB/mm and 7.1 dB/mm insertion loss[21]. Van Parys *et al.* introduced a semiconductor optical amplifier to compensate for the loss and achieved transparency (zero insertion loss) with an injection current of 160 mA[22]. Nonreciprocal mode conversion, cut-off, resonant delocalization, and coupling have also been theoretically explored[21-27].

Unlike Faraday rotation, NRPS is implemented with magnetization perpendicular to the light propagation direction and is insensitive to birefringence. Experimental on-chip isolator demonstrations using the NRPS mechanism have utilized devices based on bonded garnet crystals as well as deposited polycrystalline films. NRPS has been exploited for isolation using several device geometries including interferometers[28-30], micro-resonators[31, 32], and photonic crystals[33]. Each of these device configurations has its own advantages and limitations. Interferometer devices feature large operation bandwidth as well as relatively good fabrication tolerance, and are thus ideal for high-speed PICs or applications involving broadband-tunable laser sources. The relatively large device footprint (several millimeters) of conventional interferometers, however, is not suitable for on-chip integration. Using a push-pull configuration can reduce the required

Downloaded From: http://proceedings.spiedigitallibrary.org/ on 02/07/2017 Terms of Use: http://spiedigitallibrary.org/ss/termsofuse.aspx

device size by half, but it complicates the magnetic design as the two interferometer arms need to be magnetized in opposite directions. On the other hand, optical resonator based isolators claim much reduced device footprint by capitalizing on the effectively "folded" optical path in a resonator. Nevertheless, resonator isolators suffer from small operation bandwidth (usually a few GHz), stringent fabrication tolerance requirements, and high sensitivity to environmental perturbations (e.g., temperature fluctuations).

Besides magneto-optics, optical nonreciprocity can also be attained by non-magnetic approaches such as indirect interband photonic transitions[34-36] and optical nonlinear effects[37-39]. However, nonlinear reciprocal devices cannot provide isolation for arbitrary backward-propagating noise and therefore cannot be used as isolators[40].

In this article, we will discuss our ongoing progress in material development and device engineering towards enabling a monolithically integrated, high-performance magneto-optical nonreciprocal photonics platform[41-49], in particular focusing on a recently demonstrated single-step growth technique and device results based on the resulting material. The monolithic magneto-optical oxide growth methods are discussed in the next section. Isolator demonstration using the Ce:YIG material is described in Section 3. In the last section, we will provide a quantitative isolator performance analysis based on our experimentally measured material parameters.

2. MATERIAL DEVELOPMENT

We have established Ce:YIG growth method uses a two-step deposition process to stabilize the garnet phase and reduce the fabrication thermal budget of Ce:YIG films. Firstly a thin YIG buffer layer was deposited by pulsed laser deposition (PLD). The as-deposited amorphous YIG film was rapid thermal annealed (RTA) to crystallize into YIG phase. This thin YIG layer is necessary for forming the magneto-optically active garnet phase, as YIG crystallizes much faster than Ce:YIG and thus can function as a template for subsequent Ce:YIG growth. A second layer of Ce:YIG was deposited on the first layer by PLD followed by another annealing step. This versatile technique allows Ce:YIG growth on a varieties of substrates such as silicon, SiO_2, and silicon nitride. Films grown using this technique exhibit high magneto-optical activity: for example, we have shown that Ce:YIG film grown on silicon nitride at a slow deposition rate has an Faraday Rotation (FR) up to 2,650 deg/cm, approaching the single crystal value of 3,300 deg/cm. The two-step growth protocols have also been implemented in sputtering deposition to obtain polycrystalline Ce:YIG films[50].

While the aforementioned growth method is capable of producing high-quality Ce:YIG films, it involves two separate deposition and annealing steps which severely limits the processing throughput. Here we describe an alternative PLD method for making Ce:YIG films on a variety of substrates in which a YIG layer acts as an in situ seed layer for Ce:YIG during the crystallization of both YIG and Ce:YIG[42]. Layers of both YIG and Ce:YIG are deposited in one step followed by an anneal. Crystallization of the Ce:YIG during RTA is facilitated by YIG layer(s) on top of or at the bottom of the stack. This simplifies the process flow because only one deposition step is required instead of two and leads to films with good magnetic and MO properties. The finding that a YIG overlayer can promote Ce:YIG crystallization as well as a conventional YIG underlayer enables Ce:YIG to be grown directly on a waveguide, maximizing its interaction with the guided light without the spacing loss caused by a weakly magneto-optical YIG underlayer.

Downloaded From: http://proceedings.spiedigitallibrary.org/ on 02/07/2017 Terms of Use: http://spiedigitallibrary.org/ss/termsofuse.aspx

Ce:YIG and YIG films with layer structures consisting of YIG 30 nm/Ce:YIG 60 nm/substrate and Ce:YIG 60 nm/YIG 30 nm/substrate (with a total thickness of 90 nm) and trilayers YIG 30 nm/Ce:YIG 140 nm/YIG 30 nm and Ce:YIG 70 nm/ YIG 60 nm/Ce:YIG 70 nm (with a total thickness of 200 nm) were deposited on (001) silicon (Si) and Z-cut (0001) quartz (Qz) using PLD, followed by annealing. Identical layer sequences were also grown on (100) GGG substrates as references.

Figure 1 shows the XRD diffraction data for the bilayers and trilayers after RTA at 800 °C for 5 min. The YIG (400) peak exhibits the highest intensity in all samples on Si and Qz as shown in Figure 1a,b, which indicates that the film has a preferred (100) texture based on that of the Powder Diffraction File, in which (420) has the highest intensity. In contrast, the XRD results for the films grown on GGG after RTA are shown in Figure 1c, indicating an epitaxial single-crystal film for all layer sequences with no secondary phases. Garnet films grown and crystallized on Si and quartz are polycrystalline because there is no epitaxial relationship with the substrate. As a result, YIG (420) and (422) peaks are observed in addition to the major YIG (400) peak in Figure 1a,b. However, the garnet films on GGG (100) are lattice-matched and single-crystal, and the diffraction pattern shows YIG (h00) peaks near the GGG (h00) substrate peaks. The out-of-plane (OP) lattice constant of the films was 12.39 Å. The weak peak at 33.1 ± 0.05° for films on Si and Qz was attributed to hematite, α-Fe_2O_3, an antiferromagnet.

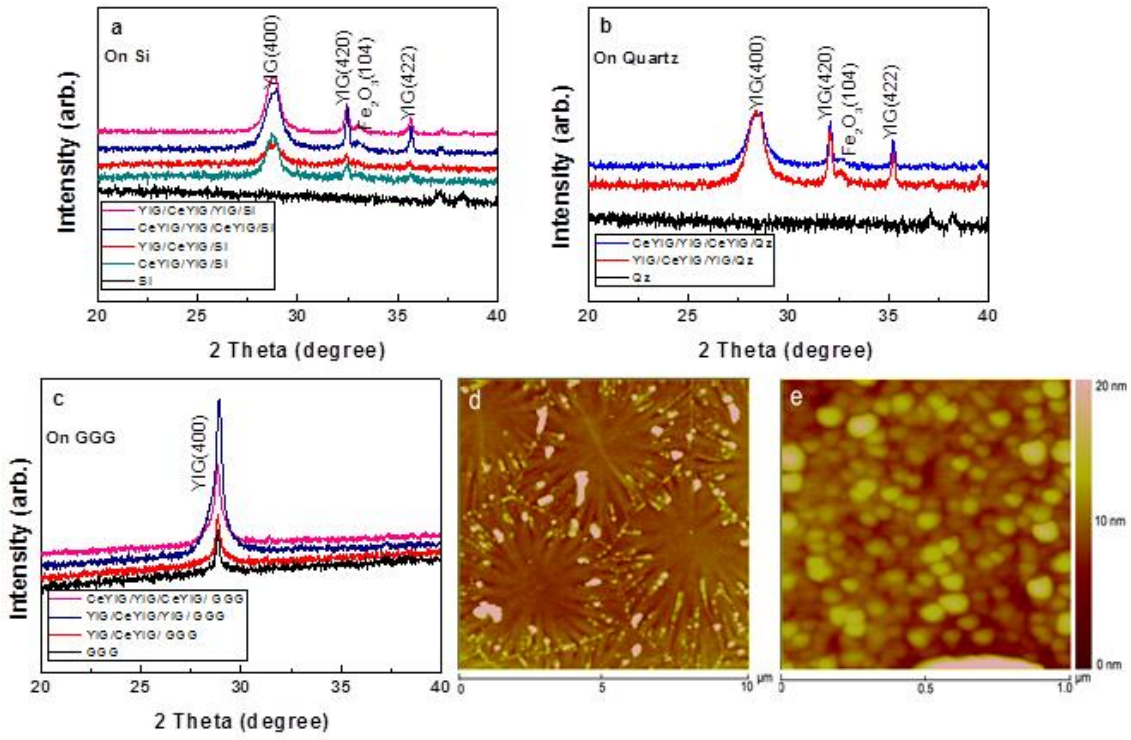


Fig. 1. XRD results and AFM images of the films on different substrates after RTA. 1D XRD ω−2θ scans for the films on (a) silicon and (b) quartz, including scans of bare substrates for comparison. (c) 1D XRD ω−2θ scans for the films on single crystal GGG (100) substrates. AFM images of (d) YIG/CeYIG/Si, 10 μm × 10 μm area, and (e) CeYIG/YIG/Si, 1 μm × 1 μm area[42].

Downloaded From: http://proceedings.spiedigitallibrary.org/ on 02/07/2017 Terms of Use: http://spiedigitallibrary.org/ss/termsofuse.aspx

The AFM surface morphology of the bilayer films on Si is shown in Figure 1d,e. For the YIG/Ce:YIG/Si, the grain size at the top surface was up to 5 μm, and the grains showed a radiating pattern, whereas in Ce:YIG/YIG/Si, dense topographic features up to ~50 nm across were visible.

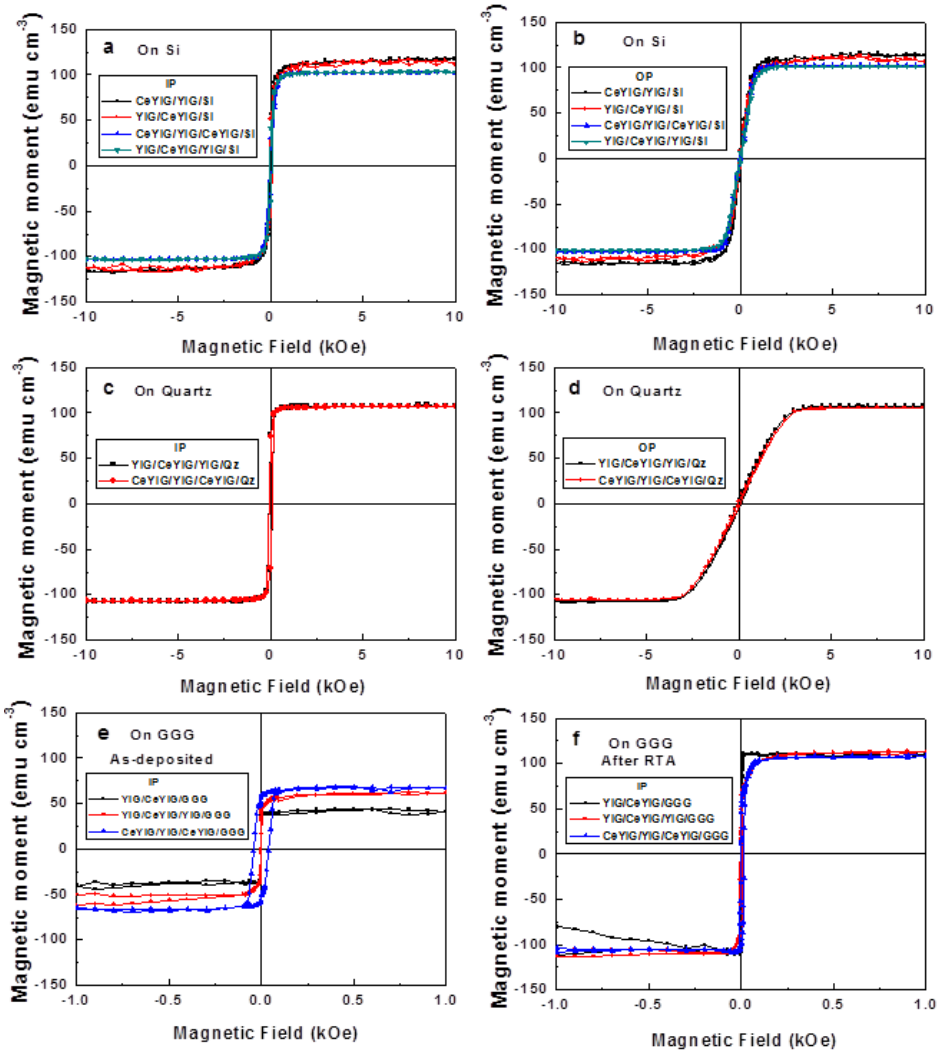


Fig. 2. Magnetic properties of the films. (a) In-plane (IP) and (b) Out-of-plane (OP) hysteresis loops of films on Si after RTA. (c) IP and (d) OP hysteresis loops of films on quartz after RTA. IP hysteresis loops of films on the single crystal GGG (100) (e) before and (f) after RTA[42].

Magnetic properties of Ce:YIG films were measured with magnetic fields applied in-plane (IP) with the film or perpendicular to the film plane (out-of-plane, OP) at room temperature using a vibrating sample magnetometer (VSM). The hysteresis loops at room temperature are given in Figure 2a–f. The saturation magnetization (M_s, averaged over all the garnet layers) of the films was 115 emu cm^{-3} (with ~5% error estimate) for the Ce:YIG/YIG/Si and 113 emu cm^{-3} for the YIG/CeYIG/Si (Figure 2a,b). The M_s of the three-layer films on Si was 103 emu cm^{-3}. The M_s of the films on Qz was about 108 emu cm^{-3} (Figure 2c,d). The M_s of the films on GGG after RTA was 110 emu cm^{-3}, as shown in Figure 2f,

Downloaded From: http://proceedings.spiedigitallibrary.org/ on 02/07/2017 Terms of Use: http://spiedigitallibrary.org/ss/termsofuse.aspx

which is higher than the unannealed values (Figure 2e). These results are consistent with the samples being primarily garnet phase without significant magnetite or maghemite spinel phases.

3. ISOLATOR DEVICE FABRICATION AND CHARACTERIZATION

In our prior work we have focused on using optical resonators as the vehicle for material magneto-optical performance quantification. The material growth and device processing techniques, however, are equally applicable to other isolator device geometries such as interferometers.

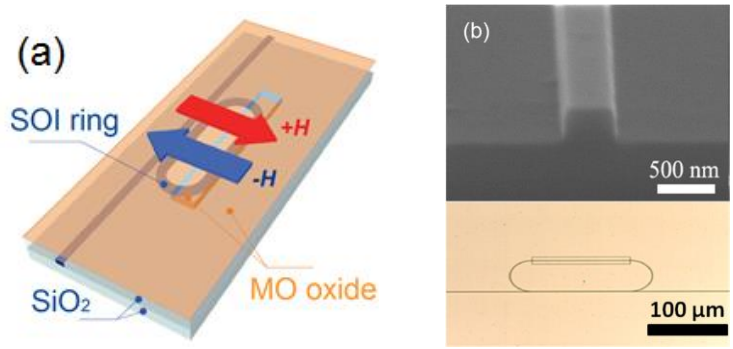


Fig. 3. (a) Schematic of the nonreciprocal optical resonator structure[41]; (b) Tilted-view SEM micrograph of the silicon-on-insulator waveguide (top) and an optical micrograph of the resonator (bottom)[42].

The resonator isolator structure used in our study operates under a homogeneously applied magnetic field. The device structure is shown in Fig. 3a. The isolator consists of a single-mode silicon racetrack resonator fabricated on an SOI wafer with a top cladding of 1-mm-thick SiO_2. Part of the SiO_2 top cladding is etched to form a 'window', which directly exposes the underlying silicon resonator waveguide surface. The magneto-optical film is subsequently deposited on the entire sample area without the need for etching.

Our prior work using films grown by the two-step technique has led to resonator isolator devices with an isolation ratio of 19.5 dB and an insertion loss of 18.8 dB[41]. The high insertion loss is attributed to excessive optical loss in the SOI/garnet waveguides (58 dB/cm, compared to 5.2 dB/cm of ChG/garnet waveguides) and consequent resonant peak broadening. Two factors contribute to this high loss: 1) the Ce:YIG film deposited on SOI waveguide sidewalls is not fully crystallized due to reduced thickness of the YIG buffer layer on the sidewalls (this cannot be resolved by simply increasing the buffer layer thickness, as the YIG/Ce:YIG film total thickness is limited by thermal expansion mismatch between garnet and the substrate); and 2) the oxide window creates two abrupt junctions between waveguide sections with and without YIG coating, resulting in significant scattering loss.

These sources of optical loss can be mitigated through careful process optimization. For example, optimized etching recipes yield vertical waveguide sidewalls can minimize deposition on the sidewalls and reduce optical loss. We have recently demonstrated a resonator isolator with much reduced insertion loss. Figure 4a and b plot the transmission spectra of quasi-transverse magnetic (TM) and quasi-transverse electric (TE) modes of the isolator, respectively,

Downloaded From: http://proceedings.spiedigitallibrary.org/ on 02/07/2017 Terms of Use: http://spiedigitallibrary.org/ss/termsofuse.aspx

measured for positive and negative magnetic fields applied in plane perpendicular to the garnet-clad section of the resonator. A resonant peak shift caused by non-reciprocal phase shift (NRPS) in the waveguide is clearly visible for the TM mode, whereas the TE mode exhibits negligible resonant peak shift, consistent with our magnetic field configuration. The device insertion loss is estimated to be (7.4 ± 1.8) dB, and the isolation ratio is (13 ± 2.2) dB. The insertion loss represents a significant improvement over our prior results. The resonant wavelengths obtained from the measurements are plotted in Figure 4c and d. The average peak shift from four separate measurements is (9.6 ± 4.1) pm for the TM mode and (1.7 ± 0.4) pm for the TE mode. The small drift over repeated measurements is likely a result of temperature change. Figure 4e plots the wavelength dependence of the non-reciprocal resonance shift.

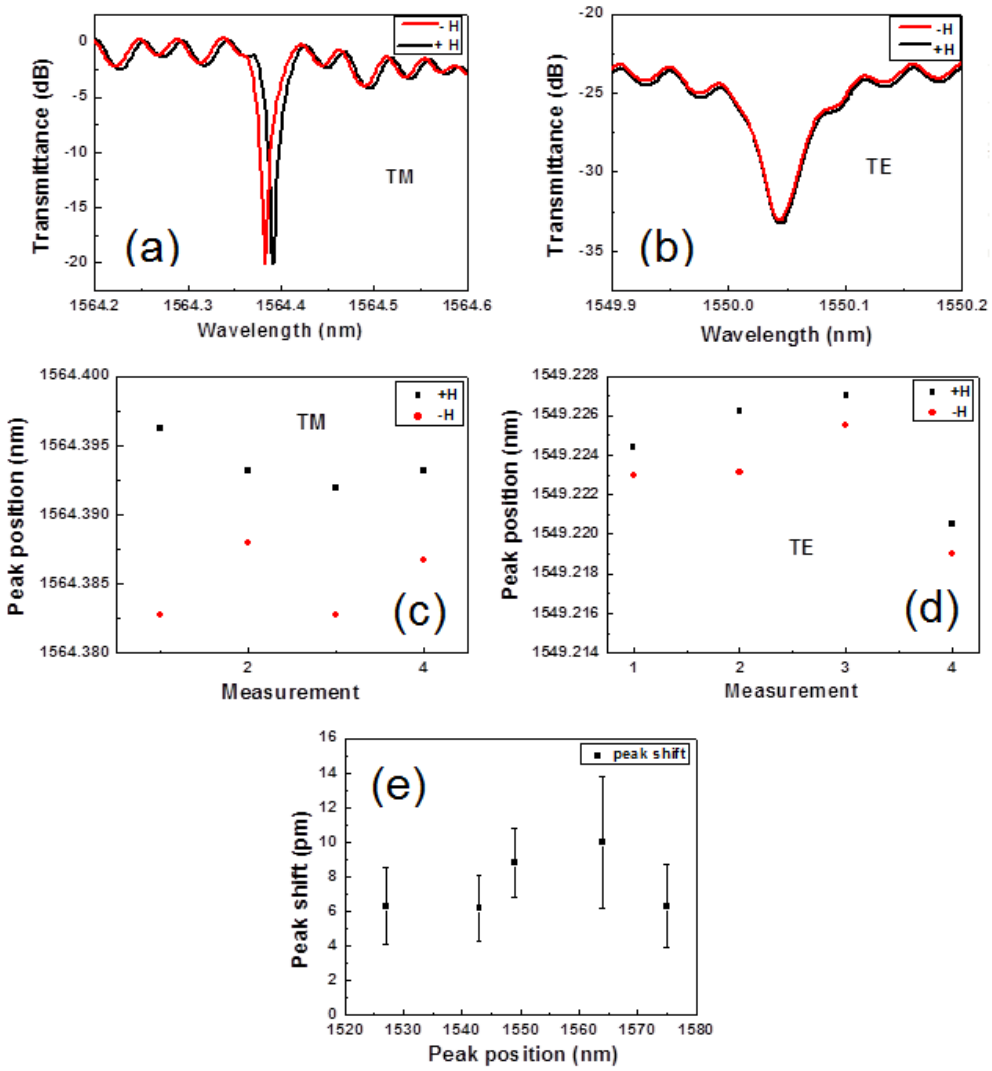


Fig. 4. (a) Transmission spectra of TM mode under applied magnetic fields of opposite directions. Insertion loss measured from the figure is 7.4 dB. (b) Transmission spectra of TE mode under applied magnetic fields of opposite directions. (c) TM mode resonant peak positions measured when the magnetic field direction was reversed ten consecutive times. (d) TE mode resonant peak positions measured when the magnetic field direction was reversed eight consecutive times. (e) Wavelength dependence of non-reciprocal resonant peak shift measured at several resonant peak locations[42].

Downloaded From: http://proceedings.spiedigitallibrary.org/ on 02/07/2017 Terms of Use: http://spiedigitallibrary.org/ss/termsofuse.aspx

5. ISOLATOR PERFORMANCE PROJECTION

The isolator device performance is closely related to the magneto-optical material figure-of-merit (FOM), which is defined as the ratio of Faraday Rotation (in deg/cm) over optical loss (in dB/cm). Here we present our modeling results quantitatively correlating the FOM with isolator device performance. Specifically, insertion loss is chosen as the device metric due to its explicit dependence on the FOM. In contrast, isolation ratio is not an intrinsic parameter reflecting the magneto-optical figure of merit of the isolator devices, because it can be maximized by approaching the critical coupling condition in micro-rings, or tuning the power splitting ratio in two interferometer arms in the case of Mach-Zehnder interferometers (MZI).

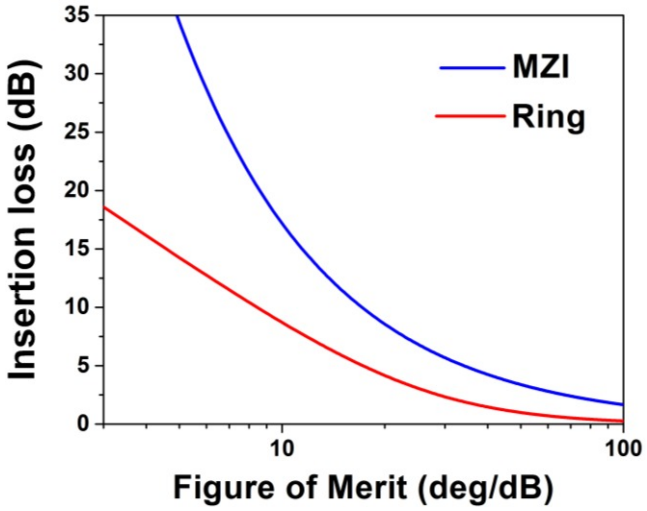


Fig. 5. Isolator insertion loss as a function of magneto-optical material FOM.

Figure 5 plots the model projection for both resonator and MZI isolators. In our model, the NRPS is maximized by choosing an appropriate SOI waveguide width. We further assume that the dominant source of optical loss results from attenuation in the magneto-optical material. The polycrystalline materials exhibit an FOM of approximately 66 deg/dB at 1550 nm wavelength, corresponding to insertion loss of 1 dB for resonator isolators and 3 dB for MZI. Material deposition and processing optimization is expected to further improve the material FOM and the isolator performance. The ultimate performance limit is set forth by the FOM of single crystalline Ce:YIG materials epitaxially grown on GGG substrates. Our recent results have demonstrated a high FOM exceeding 900 deg/dB at 1550 nm wavelength, which predicts an on-chip isolator insertion loss less than 0.3 dB.

6. SUMMARY

In conclusion, we have shown that our recently demonstrated single-step grown technique significantly improves the processing throughput and reduces the insertion loss in resulting isolator devices. Our modeling further indicates a low insertion loss of 0.3 dB is possible with optimized Ce:YIG materials. Further material engineering and device optimization are anticipated to enable high-performance monolithic optical isolation and circulation for on-chip integrated photonics.

Downloaded From: http://proceedings.spiedigitallibrary.org/ on 02/07/2017 Terms of Use: http://spiedigitallibrary.org/ss/termsofuse.aspx

7. ACKNOWLEDGEMENT

This work was supported by the National Science Foundation, MIT Lincoln Laboratories and FAME, a STARnet Center of SRC sponsored by DARPA and MARCO. This work made use of the MRSEC Shared Experimental Facilities at MIT, supported by the National Science Foundation under award number DMR-1419807.

REFERENCES

[1] Z. Yu and S. Fan, "Complete optical isolation created by indirect interband photonic transitions," Nat. Photonics **3**, 91-94 (2009).

[2] M. Scalora, J. Dowling, C. Bowden, and M. Bloemer, "The photonic band edge optical diode," J. Appl. Phys. **76**, 2023-2026 (1994).

[3] M. Soljačić, C. Luo, J. D. Joannopoulos, and S. Fan, "Nonlinear photonic crystal microdevices for optical integration," Opt. Lett. **28**, 637-639 (2003).

[4] http://www.thorlabs.com/NewGroupPage9.cfm?ObjectGroup_ID=4916

[5] http://www.newport.com/Faraday-Optical-Isolator-Free-Space/839201/1033/info.aspx

[6] T. Boudiara, B. Payet-Gervya, M. F. Blanc-Mignona, J. J. Rousseaua, M. Le Berreb, H. Joistenc, "Magnetooptical properties of yttrium iron garnet (YIG) thin films elaborated by radio frequency sputtering", J. Magn. Magn. Mat., **284**, 77-85 (2004).

[7] S. Ghosh, S. Keyvaninia, W. Van Roy, T. Mizumoto, G. Roelkens, R. Baets, "A Ce:YIG/Silicon-on-Insulator waveguide optical isolator realized by adhesive bonding," Opt. Express **20**, 1839-1848 (2012).

[8] B. Stadler and T. Mizumoto, "Integrated magnetooptical materials and isolators: a review," IEEE Photonics J. **6**, 1-15 (2014).

[9] T. Mizumoto, Y. Shoji, and R. Takei, "Direct wafer bonding and its application to waveguide optical isolators," Materials **5**, 5 (2012).

[10] M. Tien, T. Mizumoto, P. Pintus, H. Kromer, and J. Bowers, "Silicon ring isolators with bonded nonreciprocal magneto-optic garnets," Opt. Express **19**, 11740-11745 (2011).

[11] Y. Shoji, T. Mizumoto, H. Yokoi, I. Hsieh, and R. Osgood, "Magnetooptical isolator with silicon waveguides fabricated by direct bonding," Appl. Phys. Lett. **92**, 071117 (2008).

[12] T. Zaman, X. Guo, and R. Ram, "Semiconductor Waveguide Isolators," J. Lightwave Technol. **26**, 291-301 (2008).

[13] T. Zaman, X. Guo, and R. Ram, "Faraday rotation in an InP waveguide," Appl. Phys. Lett. **90**, 023514 (2007).

[14] J. Montoya, K. Parameswaran, J. Hensley, M. Allen, and R. Ram, "Surface plasmon isolator based on nonreciprocal coupling," J. Appl. Phys. **106**, 023108 (2009).

[15] K. Baba, F. Takase, and M. Miyagi, "Ferromagnetic particle composite polymer films for glass and semiconductor substrates," Opt. Comm. **139**, 35-38 (1997).

[16] K. Baba, F. Takase, and M. Miyagi, "Magnet-optic media composed of ferromagnetic metal island films for glass and semiconductor substrates," Electron. Lett. **32**, 222-224 (1996).

[17] J. Hammer, G. Evans, G. Ozgur, and J. K. Butler, "Isolators, Polarizers, and Other Optical Waveguide Devices Using a

Downloaded From: http://proceedings.spiedigitallibrary.org/ on 02/07/2017 Terms of Use: http://spiedigitallibrary.org/ss/termsofuse.aspx

Resonant-Layer Effect," J. Lightwave Technol. 22, 1754-1763 (2004).
[18] M. Levy, "The On-Chip Integration of Magnetooptic Waveguide Isolators," IEEE J. Sel. Top. Quantum Electron. **8**, 1300-1306 (2002).
[19] G. F. Dionne, G. Allen, P. Haddad, C. A. Ross, and B. Lax, "Circular Polarization and Nonreciprocal Propagation in Magnetic Media," Lincoln Laboratory Journal **15**, 323-340 (2005).
[20] D. Hutchings, B. Holmes, C. Zhang, P. Dulal, A. Block, S. Sung, N. Seaton, and B. Stadler, "Quasi-Phase-Matched Faraday Rotation in Semiconductor Waveguides With a Magnetooptic Cladding for Monolithically Integrated Optical Isolators," IEEE Photon. J. **5**, 6602512 (2013).
[21] H. Shimizu and Y. Nakano, "Fabrication and characterization of an InGaAsP/InP active waveguide optical isolator with 14.7 dB/mm TE mode nonreciprocal attenuation," J. Lightwave Technol. **24**, 38-43 (2006).
[22] W. Van Parys, D. Van Thourhout, R. Baets, B. Dagens, J. Decobert, O. Le Gouezigou, D. Make, R. Vanheertum, and L. Lagae, "Low-loss, InP-based integrated optical isolators," CLEO, paper CThC4 (2008).
[23] T. Shintaku, "Integrated optical isolator based on efficient nonreciprocal radiation mode conversion," Appl. Phys. Lett. **73**, 1946-1948 (1998).
[24] H. Hemme, H. Dötsch, and P. Hertel, "Integrated optical isolator based on nonreciprocal-mode cut-off," Appl. Opt. **29**, 2741-2744 (1990).
[25] L. Tang, S. Drezdzon, and T. Yoshie, "Single-mode waveguide optical isolator based on direction-dependent cutoff frequency," Opt. Express **16**, 16202-16208 (2008).
[26] R. El-Ganainy, P. Kumar, and M. Levy, "On-chip optical isolation based on nonreciprocal resonant delocalization effects," Opt. Lett. **38**, 61-63 (2013).
[27] J. Hammer, G. Ozgur, G. Evans, and J. Butler, "Integratable 40 dB optical waveguide isolators using a resonant-layer effect with mode coupling," J. Appl. Phys. **100**, 103103 (2006).
[28] H. Yokoi, T. Mizumoto, and Y. Shoji, "Optical nonreciprocal devices with a silicon guiding layer fabricated by wafer bonding," Appl. Opt. **42**, 6605-6612 (2003).
[29] J. Fujita, M. Levy, R. Osgood, L. Wilkens, and H. Dötsch, "Waveguide optical isolator based on Mach-Zehnder interferometer," Appl. Phys. Lett. **76**, 2158-2160 (2000).
[30] Y. Shoji and T. Mizumoto, "Ultra-wideband design of waveguide magnetooptical isolator operating in 1.31 μm and 1.55 μm band," Opt. Express **15**, 639-645 (2007).
[31] N. Kono, K. Kakihara, K. Saitoh, and M. Koshiba, "Nonreciprocal microresonators for the miniaturization of optical waveguide isolators," Opt. Express **15**, 7737-7751 (2007).
[32] H. Zhu and C. Jiang, "Optical Isolation Based on Nonreciprocal Micro-Ring Resonator," J. Lightwave Technol. **29**, 1647-1651 (2011).
[33] N. Kono and M. Koshiba, "Three-dimensional finite element analysis of nonreciprocal phase shifts in magneto-photonic crystal waveguides," Opt. Express **13**, 9155-9166 (2005).
[34] Z. Yu and S. Fan, "Integrated nonmagnetic optical isolators based on photonic transitions," IEEE J. Sel. Top. Quantum Electron. **16**, 459-466 (2010).
[35] H. Lira, Z. Yu, S. Fan, and M. Lipson, "Electrically driven nonreciprocity induced by interband photonic transition on a silicon chip," Phys. Rev. Lett. **109**, 033901 (2012).
[36] K. Gallo, G. Assanto, K. Parameswaran, M. Fejer, "All-optical diode in a periodically poled lithium niobate waveguide," Appl. Phys. Lett. **79**, 314-316 (2001).

Downloaded From: http://proceedings.spiedigitallibrary.org/ on 02/07/2017 Terms of Use: http://spiedigitallibrary.org/ss/termsofuse.aspx

[37] Z. Yu, F. Xu, X. Lin, X. Song, X. Qian, Q. Wang, and Y. Lu, "Tunable broadband isolator based on electro-optically induced linear gratings in a nonlinear photonic crystal," Opt. Lett. **35**, 3327-3329 (2010).

[38] M. Krause, H. Renner and E. Brinkmeyer, "Optical isolation in silicon waveguides based on nonreciprocal Raman amplification," Electron. Lett. **44**, 691-693 (2008).

[39] L. Fan, J. Wang, L. T. Varghese, H. Shen, B. Niu, Y. Xuan, A. M. Weiner, and M. Qi, "An all-silicon passive optical diode," Science **335**, 447-450 (2012).

[40] Y. Shi, Z. Yu, and S. Fan, "Limitations of nonlinear optical isolators due to dynamic reciprocity," Nat. Photonics **9**, 388-392 (2015).

[41] L. Bi, J. Hu, P. Jiang, D. Kim, G. Dionne, L. C. Kimerling, and C. A. Ross, "On-chip optical isolation in monolithically integrated nonreciprocal optical resonators," Nat. Photonics **5**, 758-762 (2011).

[42] X. Sun, Q. Du, T. Goto, M. Onbasli, D. H. Kim, N. Aimon, J. Hu, and C. A. Ross, "Single-step deposition of cerium substituted yttrium iron garnet for monolithic on-chip optical isolation," *ACS Photonics* **2**, 856-863 (2015).

[43] L. Bi, J. Hu, G. F. Dionne, L. C. Kimerling, and C. A. Ross, "Monolithic integration of chalcogenide glass/iron garnet waveguides and resonators for on-chip nonreciprocal photonic devices," SPIE Proc. **7941**, 794105 (2011).

[44] L. Bi, J. Hu, L. Kimerling, and C. A. Ross. "Fabrication and characterization of $As_2S_3/Y_3Fe_5O_{12}$ and $Y_3Fe_5O_{12}$/SOI strip-loaded waveguides for integrated optical isolator applications," SPIE Proc. **7604**, 760406 (2010).

[45] L. Bi, J. Hu, P. Jiang, H. S. Kim, D. H. Kim, M. C. Onbasli, G. F. Dionne, and C. A. Ross, "Magneto-optical thin films for on-chip monolithic integration of non-reciprocal photonic devices," Materials **6**, 5094-5117 (2013).

[46] L. Bi, H. Kim, J. Hu, L. C. Kimerling, and C. A. Ross, "As_2S_3/Sr $(Ti_{0.7}Co_{0.3})O_3$ and $As_2S_3/Sr(Ti_{0.6}Fe_{0.4})O_3$ strip-loaded waveguides for integrated magneto-optical isolator applications," SPIE Proc. **7218**, 721803 (2009).

[47] T. Goto, M. C. Onbaşlı, and C. A. Ross, "Magneto-optical properties of cerium substituted yttrium iron garnet films with reduced thermal budget for monolithic photonic integrated circuits," Opt. Express **20**, 28507-28517 (2012).

[48] M. C. Onbaşlı, T. Goto, X. Sun, N. Huynh, and C. A. Ross, "Integration of bulk-quality thin film magneto-optical cerium-doped yttrium iron garnet on silicon nitride photonic substrates," Opt. Express **22**, 25183-25192 (2014).

[49] T. Goto, M. C. Onbaşlı, D. H. Kim, V. Singh, M. Inoue, L. C. Kimerling, and C. A. Ross, "A nonreciprocal racetrack resonator based on vacuum-annealed magnetooptical cerium-substituted yttrium iron garnet," Opt. Express **22**, 19047-19054 (2014).

[50] P. Hansen and J. Krumme, "Magnetic and magneto-optical properties of garnet films," Thin Solid Films **114**, 69-107 (1984).

[51] A. Block, P. Dulal, B. Stadler, N. Seaton, "Growth Parameters of Fully Crystallized YIG, Bi:YIG, and Ce:YIG Films With High Faraday Rotations," IEEE Photonics J. **6**, 0600308 (2014).

Downloaded From: http://proceedings.spiedigitallibrary.org/ on 02/07/2017 Terms of Use: http://spiedigitallibrary.org/ss/termsofuse.aspx